



Article

Assessment of Accident-Tolerant Fuel with FeCrAl Cladding Behavior Using MELCOR 2.2 Based on the Results of the QUENCH-19 Experiment

Tereza Abrman Marková ¹, Guglielmo Lomonaco ^{2,3,*} , Guido Mazzini ⁴ and Martin Ševeček ¹ 

- ¹ Faculty of Nuclear Sciences and Physical Engineering, Czech Technical University in Prague, 115 19 Prague, Czech Republic; tereza.abrmanmarkova@suib.cz (T.A.M.); martin.sevecek@fjfi.cvut.cz (M.Š.)
- ² GeNERG TEC Division, DIME-Dipartimento di Ingegneria Meccanica, Energetica, Gestionale e dei Trasporti, Università Degli Studi di Genova, Via All'Opera Pia 15/A, 16145 Genoa, Italy
- ³ Istituto Nazionale di Fisica Nucleare (INFN), Sezione di Genova, Via Dodecaneso 33, 16146 Genoa, Italy
- ⁴ Department of Nuclear Safety Analyses, National Radiation Protection Institute (SURO), 140 00 Prague, Czech Republic; guido.mazzini@suro.cz
- * Correspondence: guglielmo.lomonaco@unige.it

Abstract: To ensure the applicability of accident-tolerant fuels, their behaviors under various accidental conditions must be assessed. While the dependences of the behavior of single physical parameters can be investigated in single- or separate-effect experiments, and more complex phenomena can be investigated using integral-effect tests, the behavior of an entire system as complex as a nuclear power plant core must be investigated using computer code modeling. One of the most commonly used computer codes for the assessment of severe accidents is MELCOR 2.2. In version 18019, the authors enabled the modeling of the behavior of the nuclear fuel with FeCrAl cladding (namely, alloy B136Y3) for the first time, using the GOX model. The ability of this model to reasonably accurately predict the behavior of FeCrAl cladding in accident conditions with quenching was verified in this work by modeling the QUENCH-19 experiment carried out in the Karlsruhe Institute of Technology on the QUENCH experimental device and by subsequent comparison of the MELCOR calculation results with the experiment. This article proves that the GOX model can be used to evaluate the behavior of FeCrAl cladding and that the results can be considered conservative.

Keywords: accident-tolerant fuels; MELCOR; QUENCH 19; FeCrAl



Citation: Marková, T.A.; Lomonaco, G.; Mazzini, G.; Ševeček, M. Assessment of Accident-Tolerant Fuel with FeCrAl Cladding Behavior Using MELCOR 2.2 Based on the Results of the QUENCH-19 Experiment. *Energies* **2023**, *16*, 2763. <https://doi.org/10.3390/en16062763>

Academic Editor: Malin Liu

Received: 30 January 2023

Revised: 6 March 2023

Accepted: 13 March 2023

Published: 16 March 2023



Copyright: © 2023 by the authors. Licensee MDPI, Basel, Switzerland. This article is an open access article distributed under the terms and conditions of the Creative Commons Attribution (CC BY) license (<https://creativecommons.org/licenses/by/4.0/>).

1. Introduction

Although research into accident-tolerant fuels (ATF) has been ongoing for more than a decade, in the light of the EU Taxonomy [1] and the recently released Complementary Climate Delegated Act to accelerate decarbonization [2], the topic of ATF has gained increased attention from the nuclear safety community.

The main purpose of this work is to illustrate the ability of MELCOR 2.2.18019 to predict the behavior of FeCrAl ATF cladding under conditions similar to those of a loss-of-coolant accident in a pressurized water reactor (PWR). In version 2.2.18019, the MELCOR authors implemented tools enabling the modelling of some ATFs, including an FeCrAl alloy (namely, alloy B136Y3) that is used as a nuclear fuel cladding. FeCrAl, as one of the most thoroughly investigated ATF claddings, was used in the QUENCH-19 experiment performed in August 2018 as the first bundle experiment with ATF cladding worldwide. The experimental results enabled, among other things, the testing of the capability of the integral computational codes to simulate FeCrAl cladding behavior and to appreciate the benefits resulting from its implementation in the operation of real nuclear power plants, enhancing the durability of the nuclear fuel in accident conditions and mitigating the consequences of such accidents. The topic of fuel behavior and, more specifically, the

assurance of the integrity of the fuel claddings is always a critical issue during reactor operations and the storage of spent fuel; a great deal of research has been carried out on this topic, especially by designing and performing ad hoc experimental campaigns [3]. Accident-tolerant fuels are commonly understood as nuclear fuels that can withstand accident conditions in the reactor core for a longer period of time than fuels with original designs or even current UO_2 + zirconium alloy nuclear fuel systems. Any new nuclear fuel concept should be evaluated against the current operational, economic, and safety requirements to assess its compliance.

The main attributes for a fuel system that demonstrate enhanced accident tolerance include notably reduced steam reaction kinetics, a lower hydrogen generation rate, and a reduction in the initial and residual stored energy in the core. Additionally, fuel thermo-mechanical properties, fuel-cladding interactions, and fission product behavior should be enhanced or kept at least at the same levels as those of currently used nuclear fuels. The behavior of the ATF claddings must be evaluated using tests conducted with standardized conditions to enable the comparison and evaluation of results of the various concepts in relation to one another and to currently used fuel and cladding materials. The experimental results can be used in computer code models [4].

Considerable effort still needs to be devoted to the study of ATF concepts, but the current research already offers promising results, particularly in the area of fuel cladding resistance against oxidation and hydriding, compared to zirconium alloy fuel cladding, under accident conditions that are more severe than the basic design conditions. In general, this refers to the conditions of the loss of appropriate cooling, and the reestablishment of cooling after a certain period of drying out the nuclear reactor core (e.g., in [5]). With these essential results, the further development of tools for predicting the behavior of large nuclear fuel systems became available.

For new specific cladding alloys or multilayer claddings, there is only a limited number of correlations in recent computer codes. Their specific behavior has been studied in several experiments. New correlations must be implemented into recent computer codes and validated. This seems to be an essential step in the ATF implementation process for many reasons, mainly related to obtaining information on the behavior of large ATF cores and comparing general behavior in accident conditions with currently used Zr-based fuel claddings.

MELCOR is an engineering-level fully integrated computer developed by Sandia National Laboratories since 1982 for the US NRC (United States Nuclear Regulatory Commission) [4]. MELCOR is mainly used for the comprehensive study of core melt accidents in LWR (PWR designs including WWERs and BWRs) as well as other reactor types, including selected Gen-IV systems in the latest versions. In MELCOR, a broad spectrum of severe accident phenomena in both boiling and pressurized water reactors is treated in a unified framework [4].

In version 2.2.18019, SNL researchers added properties and behaviors for silicon carbide SiC and FeCrAl into MELCOR's reactor core oxidation and material properties calculations as initial ATF properties.

The following key material properties and behaviors are essential for MELCOR simulations:

- Properties of the base material and its oxide, such as a function of temperature and irradiation, the melting temperature and any eutectics that may form, thermal conductivity, specific heat, density, and emissivity.
- Oxidation reactions, the oxidation rate, heat produced/consumed in the reaction, and reaction products.
- Arrhenius relationship for the parabolic oxidation rate [4].

In case of the absence of specific properties and behavior data or significant uncertainty in the data available for selected materials, MELCOR can be used to perform parametric studies [6].

2. Description of the QUENCH-19 Experiment

In the last two decades, the QUENCH experimental program at the Karlsruhe Institute of Technology (KIT) has brought significant benefits to the study of accident phenomenology, as well as providing an important experimental database for computer code validation. The list of QUENCH experiments and its main parameters can be found in [7] and an informative overview of the KIT publications on the QUENCH results and its use in [8].

The QUENCH-19 test was the first large-scale bundle test worldwide with any ATF cladding (FeCrAl(Y) alloy B136Y3). The QUENCH-15 test with ZIRLO cladding was used as the reference test with very similar bundle geometry and almost equal electric power and injection during the pre-oxidation and power transient stages [5,9].

The experimental facility is operated in two modes: a forced convection mode and a boil-off mode. In the forced-convection mode (also in QUENCH-19), superheated steam from the steam generator and superheater enters the test bundle at the bottom, together with argon. The cooling water circuits of the bundle and off-gas pipe guarantee steam and gas temperatures high enough to avoid condensation at the test section outlet and inside the off-gas pipe [9].

The experimental facility contains a test section with a test bundle with 32 test rods arranged in a square grid (Figure 1). Rods 1–24 are heated, black rods are unheated. The main features of the QUENCH-19 test bundle are presented in Table 1. Two types of rods were used for the test bundle: 24 heated rods with the FeCrAl(Y) alloy B136Y3 cladding provided by ORNL (see the geometry in Figure 2) and 8 unheated rods with the Kanthal APM cladding. FeCrAl(Y) alloy B136Y3 cladding's heat capacity is approximately $460 \text{ J}/(\text{Kg}\cdot\text{K})$; it has heat conductivity of approximately $11 \text{ W}/(\text{m}\cdot\text{K})$, and its melting point is approximately $1520 \text{ }^\circ\text{C}$ [10].

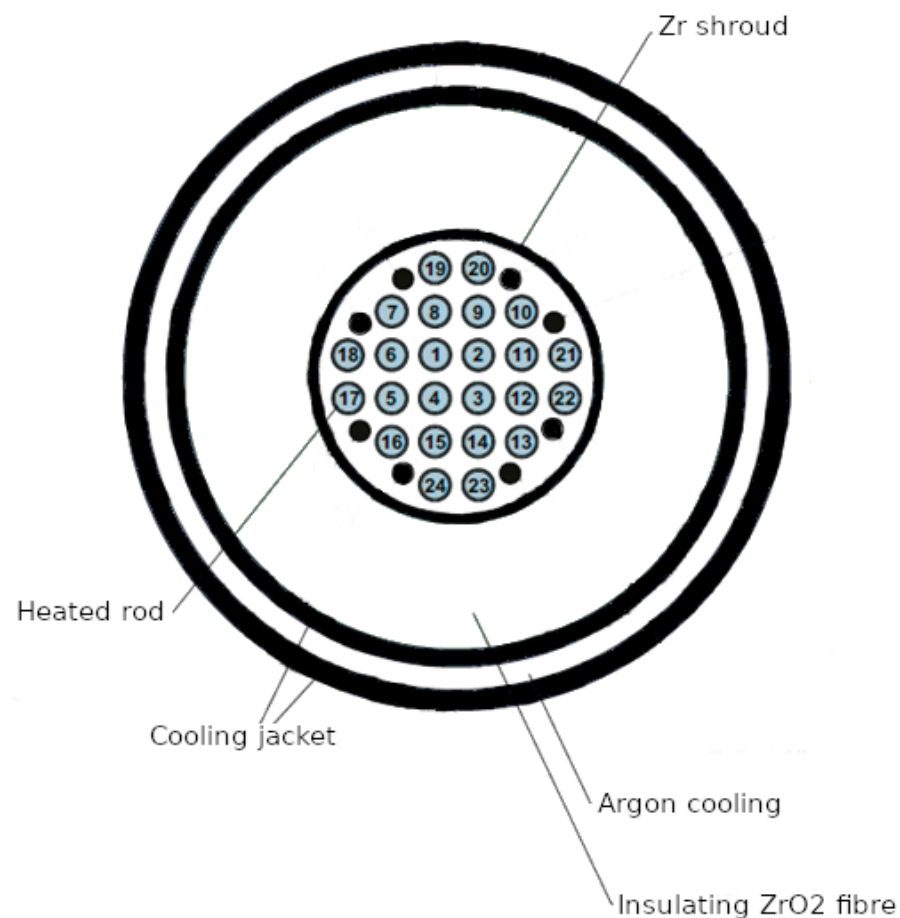


Figure 1. Cross-section of the test bundle [5].

Table 1. Parameters of the QUENCH 19 test bundle [5].

Pitch	12.6 mm
Channel area	34.57 cm ²
Hydraulic diameter	12.27 mm
Number of heated rods	24
Cladding outside diameter	9.52 ± 0.04 mm
Cladding material—heated rods	B136Y3 (Fe-6.2Al-13Cr-0.03Y)
Cladding thickness	381 µm
Full rod elevations	−690 to 1790 mm
Material of main heater	W
W heater length	1024 mm
W heater diameter	5 mm
Annular pellet material	ZrO ₂ ; Y ₂ O ₃ -stabilized
Annular pellet outside diameter	8.58 mm
Annular pellet inside diameter	5.2 mm
Pellet stack elevations	0 mm to 1024 mm
Internal rod gas, pressure	Kr, 0.22 MPa abs.
Number of unheated rods	8
Cladding material—unheated rods	Kanthal APM (Fe-5.8Al-22Cr)
Spacer grids material	Inconel (1), Kanthal (4)
Spacer grids elevation	−200; 50; 550; 1050, 1410 mm
Shroud material	Kanthal APM
Shroud wall thickness	3.03 ± 0.15 mm
Shroud inside diameter	83 mm
Shroud outside diameter	89 mm
Shroud elevation	−300 mm to 1300 mm
Shroud insulation material	ZrO ₂ fiber
Shroud insulation thickness	approx. 34 mm
Mo heaters and copper electrodes upper parts	766 mm (576 Mo, 190 mm Cu)
Mo heaters and copper electrodes lower parts	690 mm (300 Mo, 390 mm Cu)
Mo heaters and copper electrodes diameter	8.0 mm
Cooling jacket material	Inconel 600/SS
Cooling jacket inner tube dimensions	158.3/168.3 mm
Cooling jacket outer tube dimensions	181.7/193.7 mm

The test bundle, corner rods, shroud, and cooling jackets are equipped with thermocouples attached to the outer surface of the claddings. The thermocouples' uncertainties are summarized in Table 2. Hydrogen release is analyzed by a quadrupole mass spectrometer Balzers "GAM300" with the sampling position located in the off-gas pipe of the QUENCH test facility. The mass production rate of hydrogen, as well as that of the other gases, is calculated with the ratio of the concentration of the particular gas measured using ion currents and that of argon and multiplied by the argon flow rate through the test bundle [5]. Due to the lack of precise data from the benchmark [5], it is assumed that the Balzer 'GAM300' spectrometer was calibrated according to the proper methodology before the experimental measurements, and that the calibration does not influence the results. Taking into account

the accuracy of the Balzer ‘GAM300’ spectrometer of 0.1% during flow measurements, as shown in [11], and using basic assumptions regarding the integration of measurement uncertainties, the expected uncertainty for the sum of H₂ produced during the experiment is approximately ± 0.5 g.

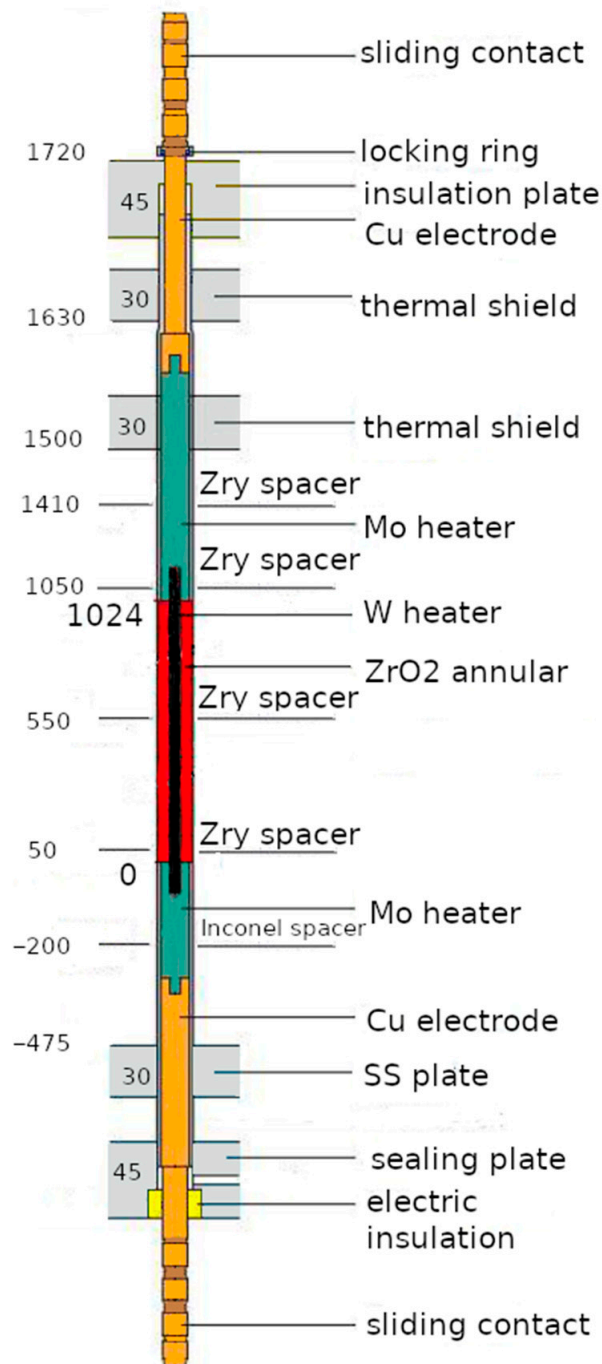


Figure 2. Heated rod geometry, axial view [5].

Table 2. Thermocouples’ uncertainties [5].

Bundle Elevation	Thermocouple Type	Uncertainty Low Temperatures	Uncertainty High Temperatures
0–500 mm	NiCr, Ni	± 2 K up to 600 K	$\pm 0.005 \times T$ [K] above 600 K
600–1300 mm	W, Re	± 5 K up to 700 K	$\pm 0.01 \times T$ [K] above 700 K

The QUENCH-19 experimental sequence was divided into the following stages:

- Pre-oxidation, 0–6018 s
- Heat-up, 6018–7127 s
- Extended period, 7127–9100 s with constant electrical power
- Quench \approx 9115–9285 s with water flow rate 48 g/s

The end of the measurement was at 10,280 s. The inlet steam and argon temperature were 640–700 K, the pressure was 0.22 MPa, the steam flowrate was 2.4–3.9 g/s, the argon flowrate was 3.5 g/s, the quenching water temperature was 299 K, and the flowrate was 44–46 g/s [12].

During the post-test disassembly of the bundle, about 7300 g of water leaked from the annulus between the shroud and the cooling jacket, and the post-test weighting of humid heat insulation showed that about 400 g was collected in insulation pores [5]. The leakage was neglected in this work for the ease of comparing future results with the QUENCH-15 experimental calculation results.

During the test, two KANTHAL APM corner rods were withdrawn and, during the post-test investigation, only a slightly oxidized surface was observed. The post-test inspection of the peripheral rods showed the formation of cladding circumferential breaks, developed due to thermal axial expansion followed by a quench shrinkage. The first Kr release was measured at 7700 s, which indicates the first cladding failure. Extensive cladding failure was observed at 9119 s (with an internal rod pressure decrease). The claddings of most of the rods at an elevation of 850 mm remained almost undamaged.

This description of the QUENCH-19 experiments enables us to study the behavior of nuclear fuel cladding under conditions partially similar to those of loss-of-coolant accidents (LOCAs) in the PWR from the phenomenological point of view. Although the temperature ramping is slower than it is during the LOCA, the experiment enables us to assess the quenching of the overheated fuel with the maximum cladding temperatures in a range similar to that in LOCA. This is especially important for the study of ATF cladding behavior and its qualification for LOCA conditions.

3. MELCOR Model Description

A model of the QUENCH experimental device was prepared in the layout used for the QUENCH-19 experiment in MELCOR 2.2.18019. The model consists of 48 control volumes (CVH structures) and 36 flow junctions (FL structures) including 2 time-driven valves and 25 heat structures (HS) with a film tracking model for the realistic course of condensation in the calculation; see Figure 3.

A model of the heated test bundle was prepared in the COR package using 22 axial levels and 3 radial rings (Figure 4). The inner ring contained 12 heated fuel rods (numbers 1–6, 8, 9, 11, 12, 14, and 15 in Figure 1), the middle contains 12 heated rods and 8 unheated rods, and the outer ring includes the area from the shroud through the insulating layer of zirconium fibers to the cooling jacket.

The 22 axial levels are assigned to the corresponding control volumes; 1 control volume is always common for the 2 middle rings and the other is assigned to the 3rd unheated ring. The other control volumes are used as media sources for the system and as a cooling circuit. COR levels 6–15 are electrically heated. The electrical heating power was set according to the experimental data; see Figure 5.

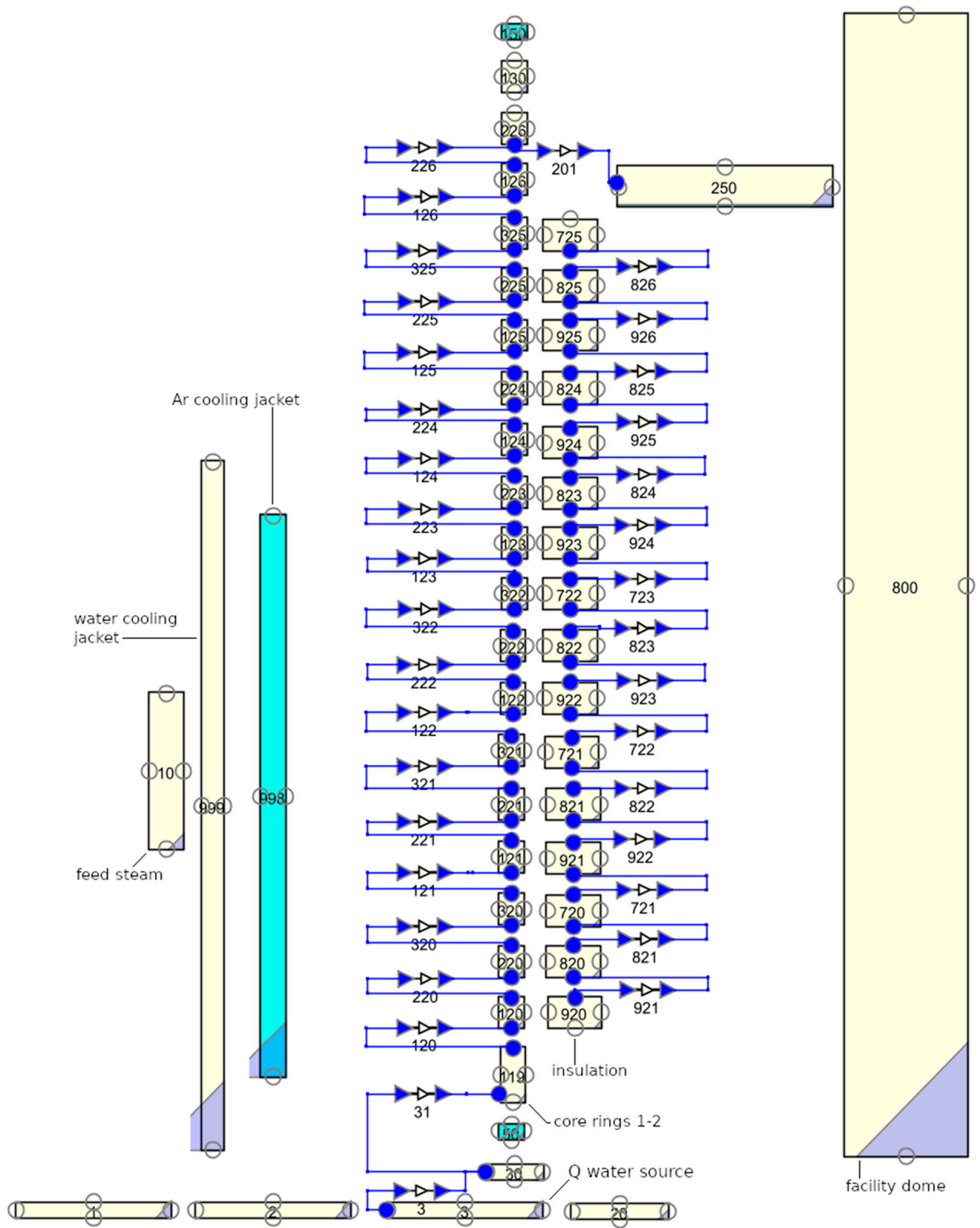


Figure 3. Model nodalization: control volumes and flow junctions.

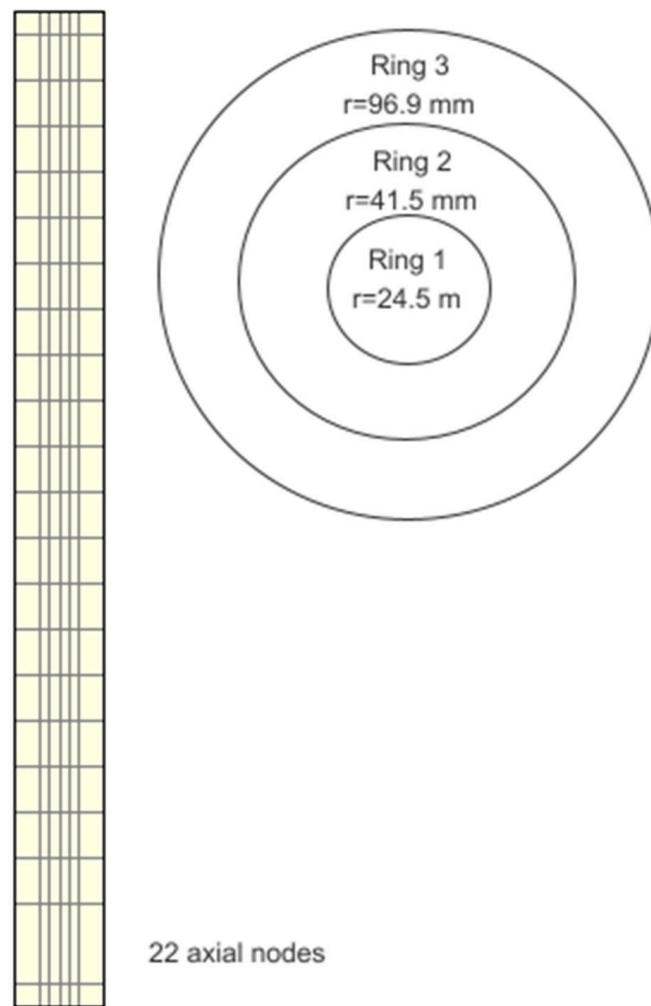


Figure 4. Model nodalization—core.

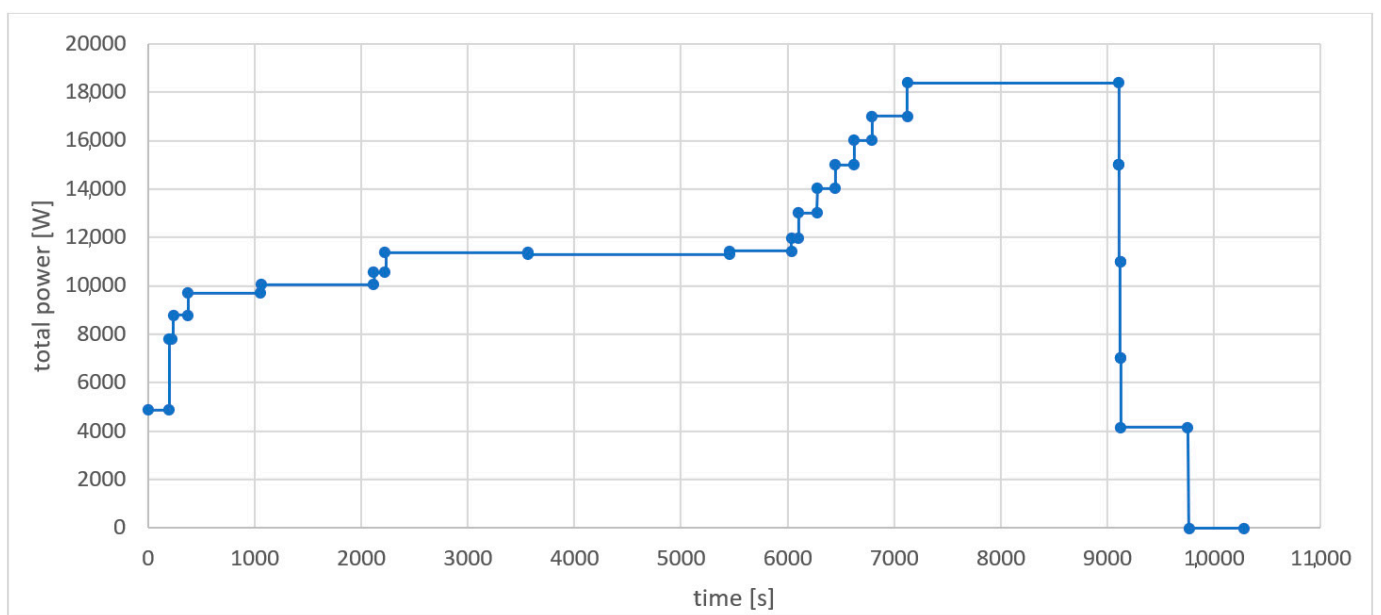
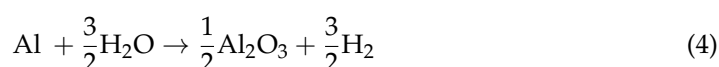
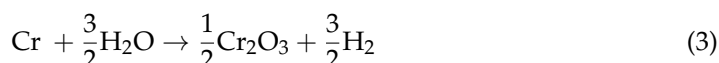
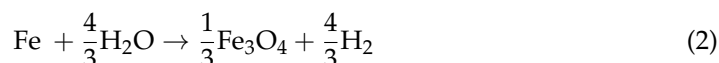


Figure 5. Test bundle electrical heating power [12].

The fuel rod material was modeled using the appropriate materials and its properties were input directly into MELCOR with a minimum number of user-defined properties. For the FeCrAl cladding modeling, the new Generic Oxidation Model (GOX) was used. This model was first implemented in MELCOR version 2.2.18019 [4]. The GOX model enables us to define the material properties of the FeCrAl alloy, as well as its oxidation equations and oxidation dynamic, and the basic properties of the produced oxides in the form of a simplified theoretic sum of FeCrAl-oxide. In the GOX model, the following basic oxidation equations are used (1)–(4) [4]:



The properties of FeCrAl Kanthal were used for the whole test bundle as it is a material that is predefined and described in the manual [4]. Even if this choice is not fully precise for the real test bundle in which the FeCrAl B136Y type was used (at least for the unheated rods), for the purpose of the work presented, it provides sufficient knowledge of the FeCrAl behavior.

The mass of oxygen absorbed by the nuclear fuel cladding and the thickness of the oxide layer formed is led by a parabolic time law (5):

$$(\Delta M_{\text{O}})^2 = K_{\text{O}}(T)\Delta t \quad (5)$$

ΔM_{O} is the mass change caused by oxygen absorbed by the cladding, and $K_{\text{O}}(T)$ is the reaction rate.

The parabolic law is a simple and commonly used approximation of the real oxidation behavior and, as such, it is also implemented in MELCOR for both Zr-based cladding oxidation and FeCrAl cladding oxidation. The rate constant $K(T)$ ($\text{kg}^2/\text{m}^4\text{s}$) as a function of temperature T (K) is calculated in MELCOR for FeCrAl by (6):

$$K(T) = C1001(7,1)e^{\left(\frac{-C1001(8,1)}{T}\right)}, T \leq C1001(10,1) \quad (6)$$

The C1001 coefficients are the sensitivity coefficients available in MELCOR for the metallic cladding oxidation rate constant, as shown in Table 3. Breakaway oxidation for FeCrAl above 1748 K is modeled using the stainless-steel reaction rates given by C1002 (steel oxidation rate constant coefficients) for H_2O , and the linear transition to breakaway oxidation from C1001(10) to C1001(9) is calculated [4]. The default values of C1001 were used for the analysis in this paper. This corrosion kinetics model is based on data from [13]. A new reaction rate correlation can be derived from recent KIT data [14]. Both reaction rates are shown in Figure 6 in comparison to the standard correlations for Zr-based cladding. The FeCrAl B136Y reaction rate shows higher oxidation rates in the low-temperature region (below 1000 °C) and earlier breakaway (above 1350 °C).

Table 3. Metallic cladding oxidation rate constant for FeCrAl in MELCOR 2.2. 18019 [4].

Coefficient Indication	Coefficient Description	Default I = 1 (H ₂ O Reaction Rates)
C1001(7,1)	Low-temperature range constant coefficient	4630 kg ² m ⁻⁴ s ⁻¹
C1001(8,1)	Low-temperature range exponential constant	41,376 K
C1001(9,1)	Upper temperature boundary for breakaway temperature range	1773 K
C1001(10,1)	Lower temperature boundary for breakaway temperature range	1748 K

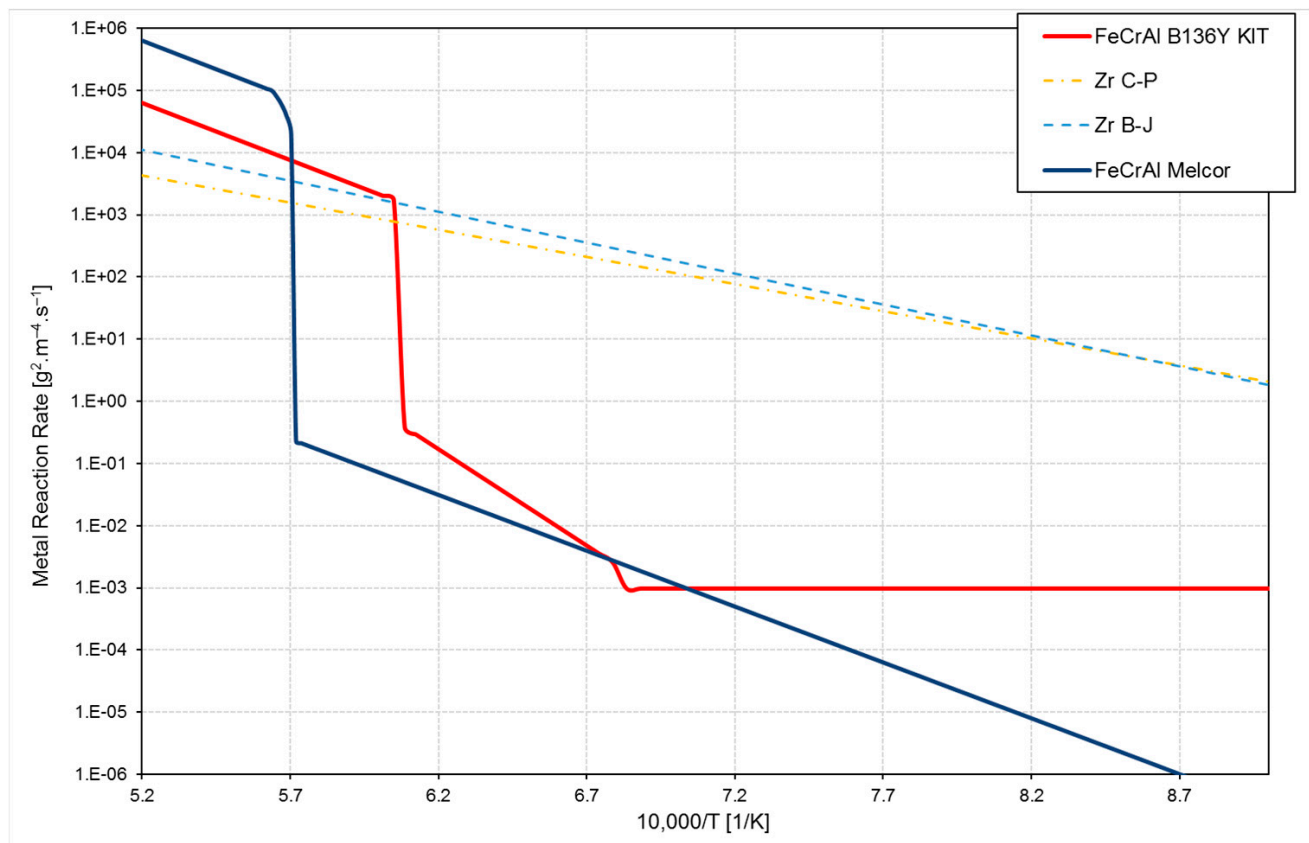


Figure 6. Metal reaction rates for cladding alloys. FeCrAl MELCOR corresponds to the parameters shown in Table 3. FeCrAl B136Y KIT is the reaction rate recently measured by KIT [14], and C-P and B-J are well-known correlations for Zr [15,16].

To stabilize the initial conditions, an initiation calculation lasting 100 s was performed.

4. Results

The comparison of the temperature trends calculated by MELCOR in the heated part of the bundle is reported in the Figure 7 for the central ring and Figure 8 for the peripheral ring. The maximum temperature of 1753 K was found at a height of 750 mm from the bottom of the heated part of the test bundle. The maximum temperatures reached in the neighboring axial position were very similar. The comparison of the temperature courses measured during the experiment is shown in Figures 9–11 (peripheral ring, rods 7, 10, 13, and 16–22 in Figure 1).

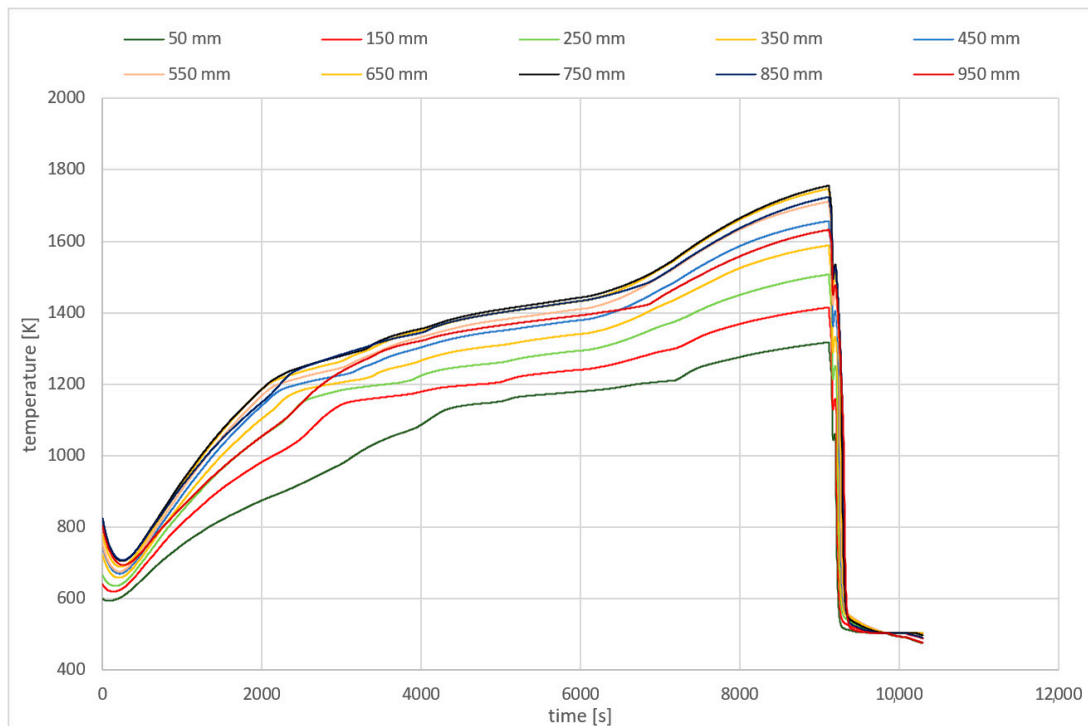


Figure 7. Temperatures calculated by MELCOR in the heated part of the bundle and the central ring (axial level, number of rings).

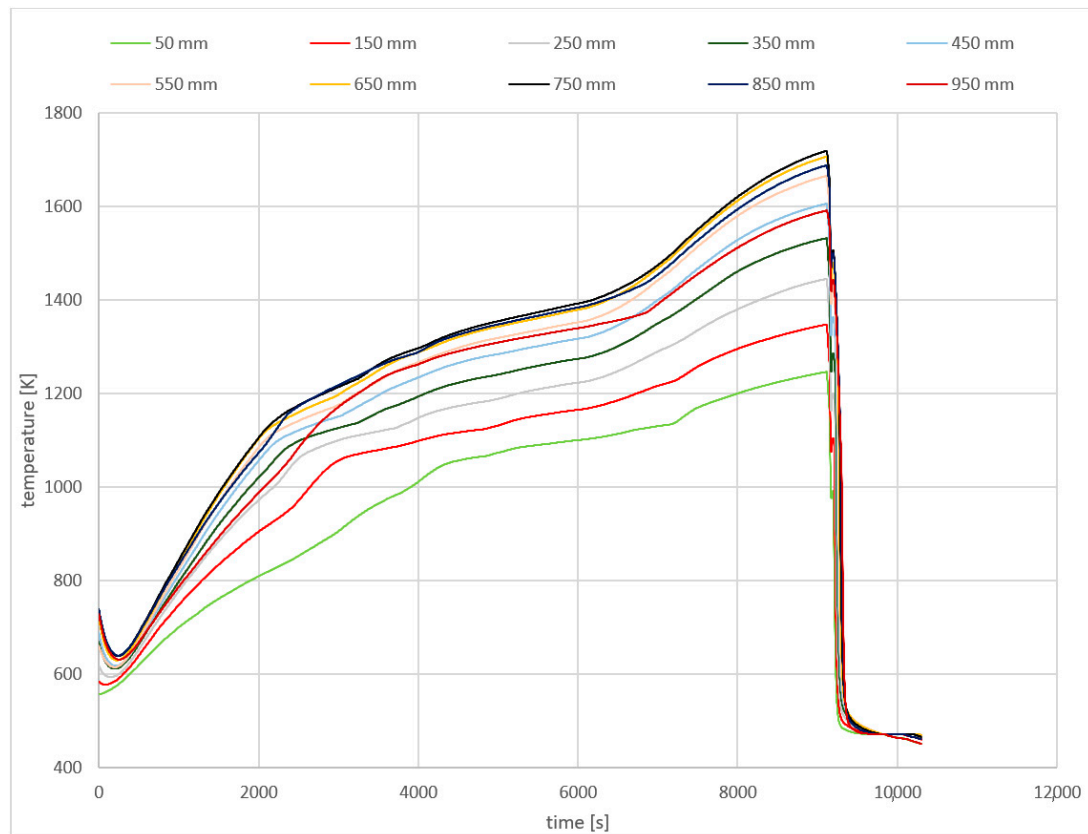


Figure 8. Temperatures calculated by MELCOR in the heated part of the bundle and the peripheral ring (axial level, number of rings).

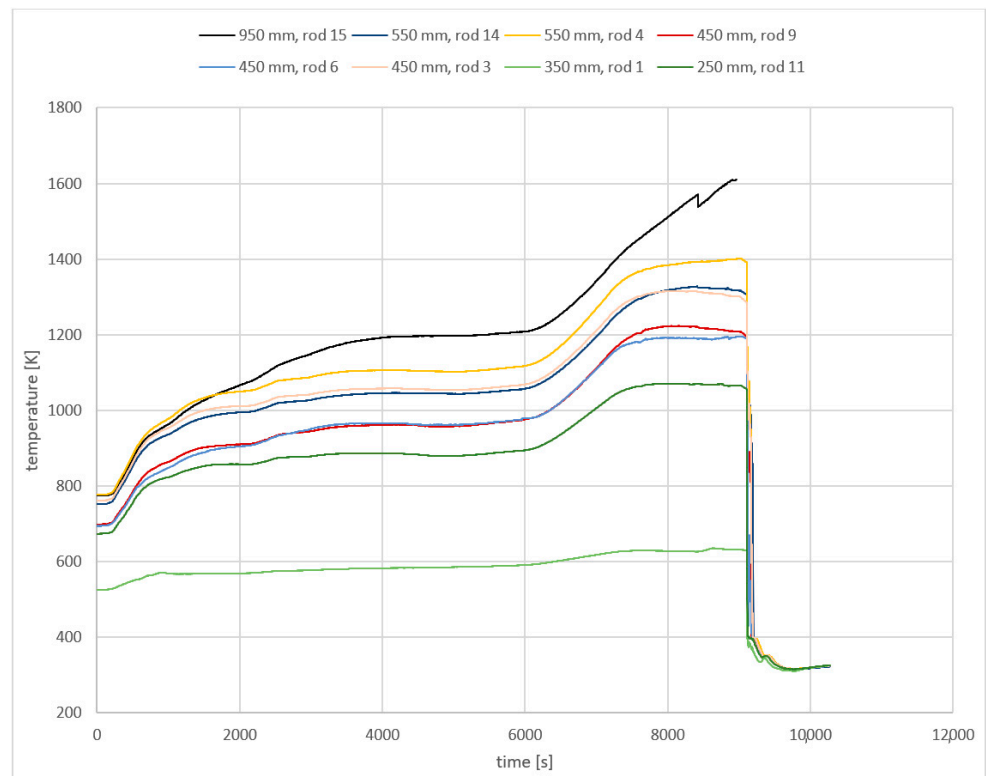


Figure 9. Temperatures measured in the heated part of the bundle and the central ring, 1/2 (axial level, rod) [12].

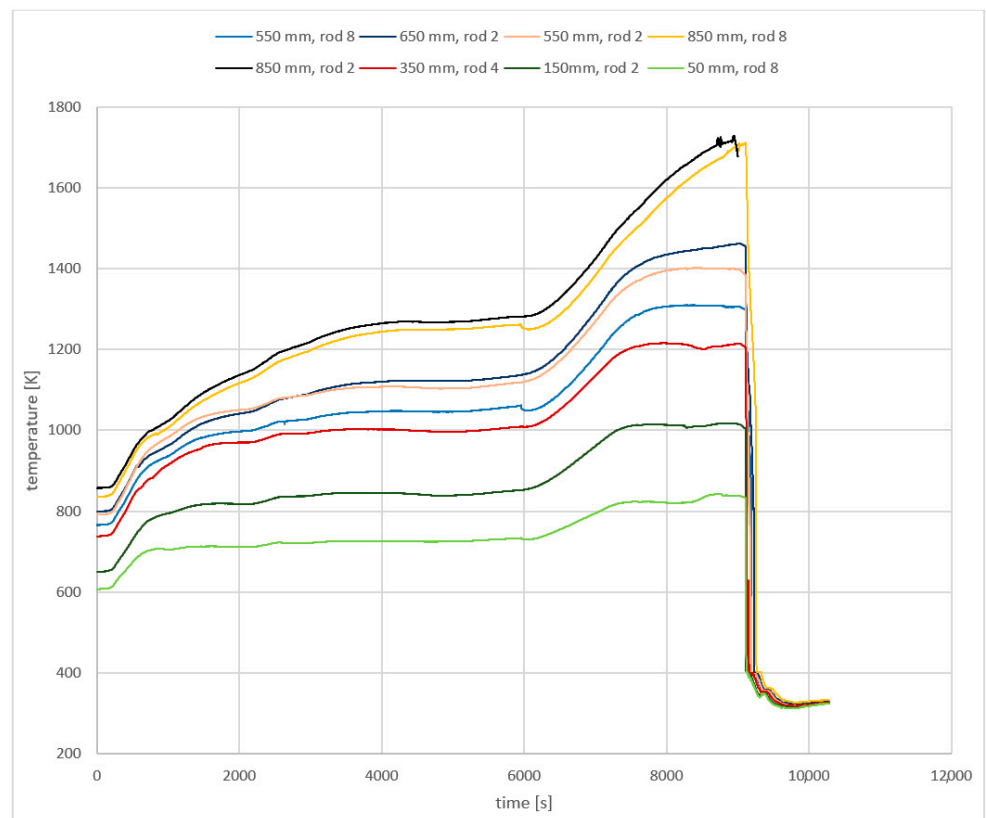


Figure 10. Temperatures measured in the heated part of the bundle and the central ring, 2/2 (axial level, rod) [12].

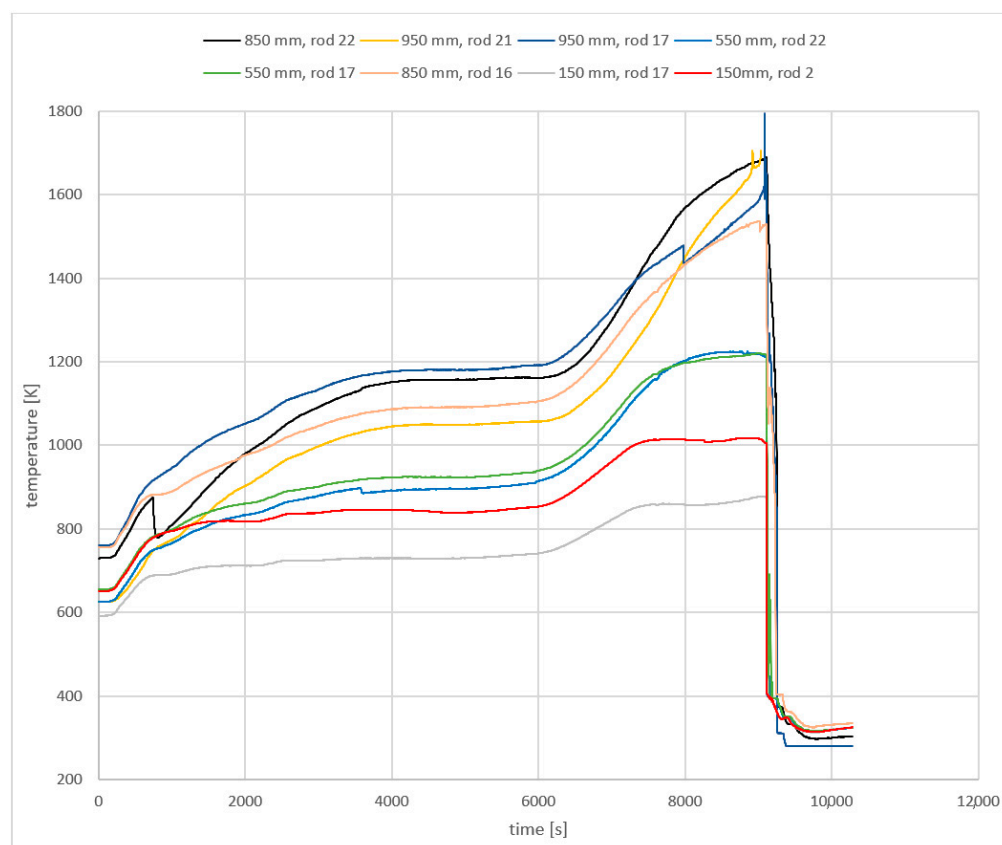


Figure 11. Temperatures measured in the heated part of the bundle and the peripheral ring (axial level, rod) [12].

The calculated and measured temperatures for the central ring of the test bundle (fuel rods 1–6, 8, 9, 11, 12, 14, and 15 in Figure 1) are compared in Figure 12. The experimental maximum of 1795 K at the height of 950 mm from the bottom of the heated part of the test bundle is not a trusted value because it is a single value that is unrealistically higher than the ambient values, as shown in Figure 13 and Table 4. This value was screened out from the results used for this work since it is probably the result of a purely computational oscillation.

After the data cleaning, the experimental maximum of 1728 K was measured at a height of 850 mm from the bottom of the heated part of the test bundle. As shown in Figure 13, two rods instrumented by the thermocouple in the appropriate axial position are compared. The difference of 25 K can be considered negligible due to the accuracy of the measurement and the sensitivity of the calculation. As shown in Figure 12, the time dependence of the temperature in the most heated parts of the experimental fuel bundle is in good agreement with the experimental results.

Figure 14 shows the time dependence of the amount of hydrogen resulting from the calculation results in comparison with the data measured in the experiment. In the experiment, a total amount of 9.25 g of hydrogen was formed. The expected measurement accuracy is approximately ± 0.5 g. The prediction of the MELCOR calculation is 14.9 g. The calculated trend is in good agreement with the experimental data. The overestimation of the total hydrogen production is acceptable from the point of view of the safety assessment, as the result is conservative. The overestimation could be caused by the use of Kanthal FeCrAl oxidation properties or by FeCrAl(Y) B136Y3 fuel rods (see Figure 6), or by simple conservatism implemented in the code.

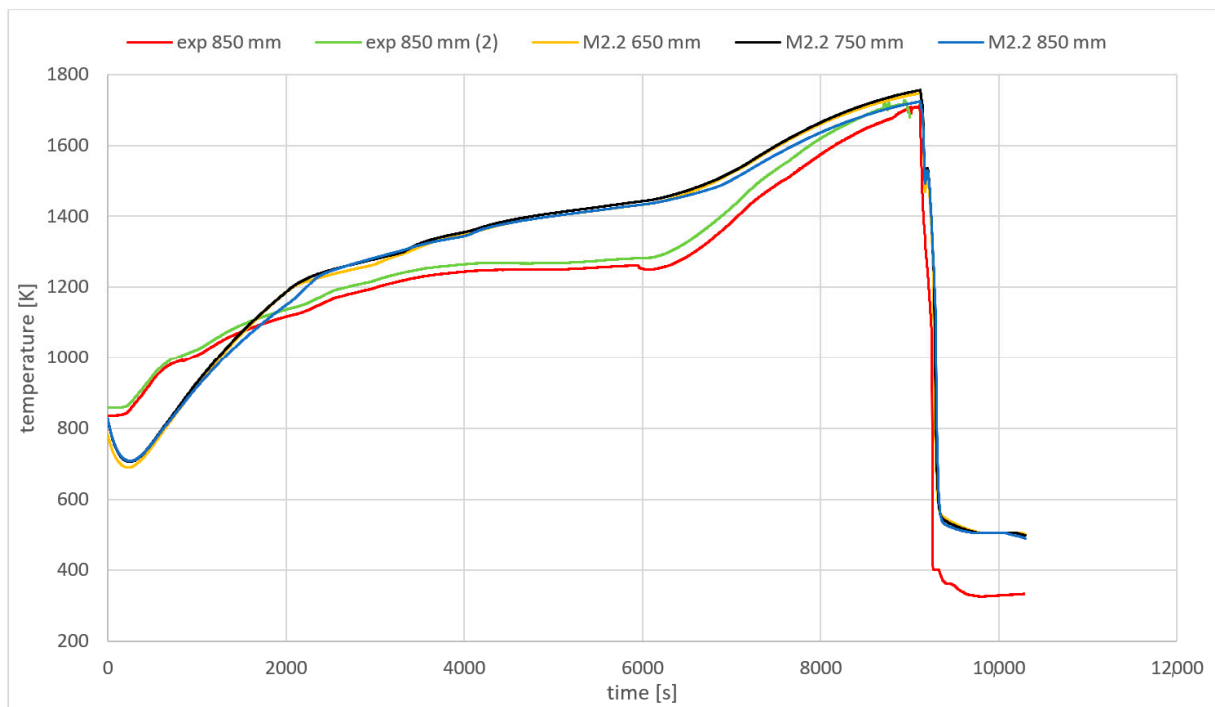


Figure 12. Comparison of the maximum temperatures of the test bundle heated rods (exp 850 mm, exp 850 mm (2)), and the central MELCOR calculation radial ring rods (M2.2 650 mm, M2.2 750 mm, M2.2 850 mm) [12].

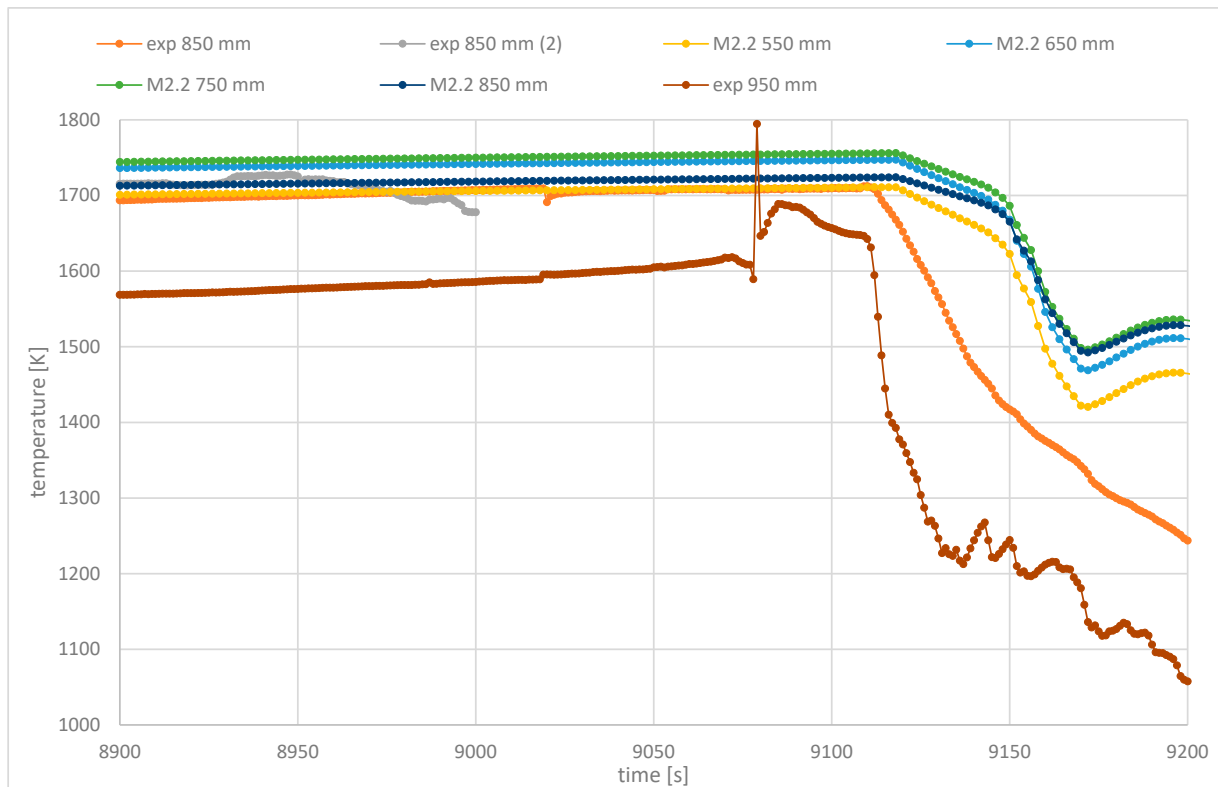


Figure 13. Temperatures measured in the heated part of the bundle, detail view 9000–9200 s (axial level, rod) [12].

Table 4. Cut-out of the measured temperature table for the axial position 950 mm of the heated rod n. 17 [12].

Time [s]	Temperature [K]
9078	1589.3
9079	1794.6
9080	1646.5

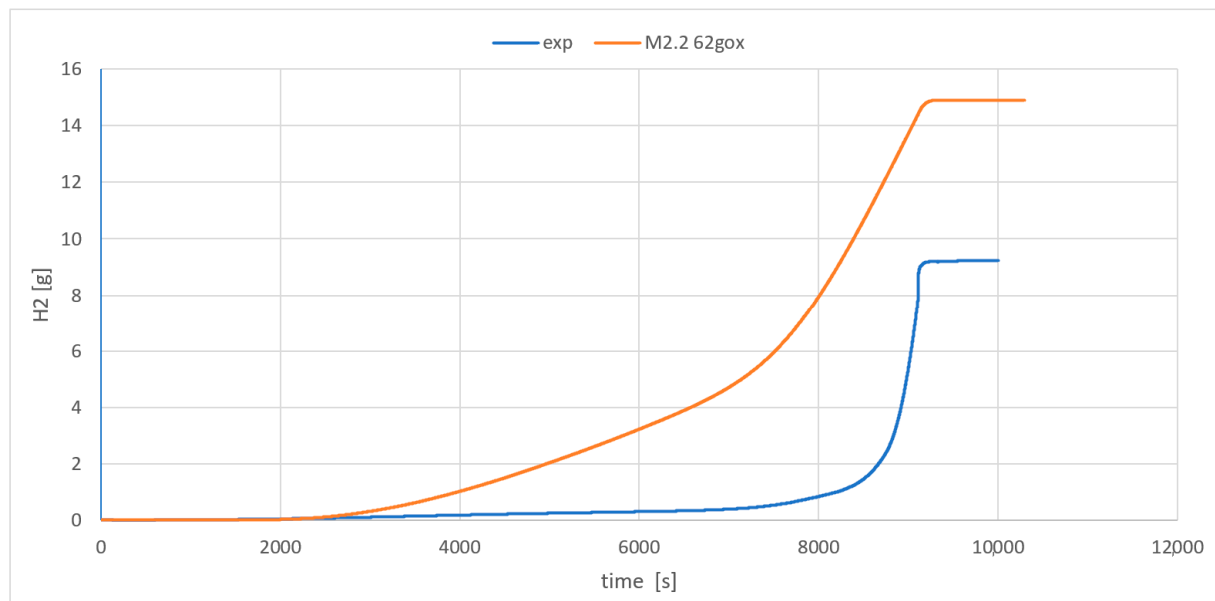


Figure 14. Comparison of the amount of hydrogen produced in the experiment and the MELCOR calculation results [12].

The GOX model is one of the newest parts of the MELCOR code; as such, it can be considered to still be under development. Currently, it is not possible to perform a sensitivity analysis on the sensitivity coefficients C1001(7,1)–C1001(10,1) for the oxidation parabolic law implemented in MELCOR using the 2.2.18019 version; this is also the case for the 2.2.21402 version, meaning that we are not able to change the above-mentioned sensitivity coefficients. A change in the C1001(7,1) and C1001(8,1) sensitivity coefficients would allow for the use of more precise data for FeCrAl(Y) B136Y3 [14], and this adjustment can be the subject of future research activities.

5. Summary

Further examination of the oxidation mechanism and kinetics of nuclear-grade FeCrAl alloys was performed in [14]. This work undertakes the important refinement of experimental values of oxidation parameters for FeCrAl(Y) B136Y3 and C26M2; these alloys have very similar compositions, with an additional amount of approximately 2% of molybdenum in the case of the C26M2 type. New separate effect tests are also performed, focusing on the high-temperature steam behavior of FeCrAl alloys to refine the values; this is also performed at FSNPE CTU, KIT, EK, and their cooperating institutions. Building on this work, these results may be used to refine the sensitivity parameters in future calculations. In addition to updating the corrosion kinetics models, two more challenges described in the experimental report remain: (1) steam leakage from the bundle into the insulation was found during post-test evaluations. This effect is not taken into account in the model, as the leakage rate and its effect on the boundary conditions are not known and are difficult to quantify. (2) It was observed that the first melting in the bundle appeared in places of contact between the thermocouples and the cladding rods. It was caused by high-temperature

material interactions between dissimilar metals and resulted in premature melting and the acceleration of the oxidation kinetics and degradation of the bundle, including additional hydrogen generation. This effect was not quantified using the model, but its contribution to the experimental results is not negligible.

Although the results of the H₂ generation in the calculations are substantially higher than the experimental results, this work showed that MELCOR can provide acceptable results with regards to this issue. This finding differs substantially from the results presented in [14], which were also obtained with the same version of MELCOR (deduced from the date of publication), where only about 5% of the experimental H₂ amount was observed. In [17], a basic comparison of the results for AC2 and ASTEC is also available. With a more sophisticated calculation of the H₂ generation in comparison with MELCOR, both AC2 and ASTEC show very good agreement with the experimental results. Considering the temperature trend and the maximum temperature value reached during the experiment, all codes are in good agreement with the experiment.

6. Conclusions

The GOX model that is newly implemented in the MELCOR 2.2 code offers us the opportunity to credibly assess FeCrAl behavior under accident conditions with an overheated fuel quenching phase, which is partially similar to LOCA. This is especially important for studies of ATF cladding behavior and its qualification, as well as providing the basis for the preliminary assessment of the overall benefits of implementing FeCrAl ATF into the PWR and its benefits in terms of severe accident assessments. Under these conditions, the different oxidation kinetics of the FeCrAl can bring a valuable additional time margin for accident mitigation and also provide additional enhancement to the resistance of the nuclear fuel cladding and H₂ management.

The study outlined in this article showed that MELCOR 2.2 is suitable for and conservative in evaluating maximum temperatures and assessing H₂ production. The GOX model is newly implemented in version 18019; however, it currently has certain limitations in terms of the use of sensitivity coefficients, which will likely be addressed by the code developers in some future versions. Further studies and development are also necessary for SMRs, in which ATF can be introduced from the beginning of the design phase. For the sensitivity assessment, it is also possible to study and compare the differences between QUENCH 19 and QUENCH 15; another KIT test was performed under conditions comparable to QUENCH 19 with ZIRLOTM nuclear fuel cladding tubes, and the results of the measurements are described in [14].

Author Contributions: Conceptualization, T.A.M., G.M. and M.Š.; Methodology, T.A.M. and M.Š.; Software, T.A.M., G.M. and M.Š.; Validation, T.A.M., G.L. and M.Š.; Formal analysis, T.A.M.; Investigation, T.A.M.; Data curation, T.A.M.; Writing—original draft, T.A.M.; Writing—review & editing, T.A.M., G.L., G.M. and M.Š.; Supervision, G.L. and G.M.; Project administration, G.M. and M.Š.; Funding acquisition, T.A.M., G.L., G.M. and M.Š. All authors have read and agreed to the published version of the manuscript.

Funding: This study was co-financed from the state budget by the Technology Agency of the Czech Republic (TAČR) within the Théta Programme, project number TK03020034, “Utilization of Advanced Materials for New Types of Nuclear Fuels”.

Data Availability Statement: The research data from this project can be shared only upon approval from the Czech Technical University, Faculty of Nuclear Sciences and Physical Engineering after meeting the conditions of Technology Agency Czech Republic, programme THETA.

Acknowledgments: The support of IAEA within the CRP “Testing and Simulation for Advanced Technology and Accident Tolerant Fuels (ATF-TS)” is acknowledged. The authors also acknowledge the valuable cooperation of Juri Stuckert of the KIT, Terttaliisa Lind of PSI for sharing the QUENCH-16 Melcor input file, and Thorsten Hollands of GRS. The main author of this paper is a Ph.D. student at the Faculty of Nuclear Sciences and Physical Engineering, Czech Technical University Prague, which

participates the above-mentioned project. Additionally, the authors would like to thank the National Radiation Protection Institute for its support during the development of the MELCOR model.

Conflicts of Interest: The authors declare no conflict of interest.

References

1. European Union. Regulation (EU) 2020/852 of the European Parliament and of the Council of 18 June 2020 on the Establishment of a Framework to Facilitate Sustainable Investment, and Amending Regulation (EU) 2019/2088, PE/20/2020/INIT. *Off. J. Eur. Union* **2020**, *198*.
2. Commission Delegated. Regulation (EU) 2022/1214 of 9 March 2022 amending Delegated Regulation (EU) 2021/2139 as regards economic activities in certain energy sectors and Delegated Regulation (EU) 2021/2178 as regards specific public disclosures for those economic activities (Text with EEA relevance), C/2022/631. *Off. J. Eur. Union* **2022**, *188*.
3. Namburi, H.K.; Ottazzi, L.; Chocholousek, M.; Lomonaco, G.; Gavelova, P.; Krejci, J. Study hydrogen embrittlement and determination of E110 fuel cladding mechanical properties by ring compression testing. *IOP Conf. Ser. Mater. Sci. Eng.* **2018**, *461*, 012059. [[CrossRef](#)]
4. Humphries, L.; Beeny, B.; Gelbard, F.; Louie, D.; Phillips, J. *MELCOR Computer Code Manuals Volume 1: Primer and Users' Guide Version 2.2.18019 2021*; Sandia National Laboratories: Albuquerque, NM, USA, 2021.
5. Stuckert, J.; Große, M.; Steinbrück, M. *Results of the Bundle Test QUENCH-19 with FeCrAl Claddings*; Institut für Angewandte Materialien, Angewandte Werkstoffphysik, Karlsruher Institut für Technologie: Karlsruhe, Germany, 2022.
6. OECD. Nuclear Energy Agency Organisation for Economic Co-operation and Development. In *State-of-the-Art Report on Light Water Reactor Accident-Tolerant Fuels*, NEA No. 7317; OECD: Paris, France, 2018.
7. Karlsruhe Institute of Technology. QUENCH Test Matrix. 2023. Available online: <https://quench.forschung.kit.edu/24.php> (accessed on 30 January 2023).
8. Karlsruhe Institute of Technology. Reports QUENCH. 2023. Available online: <https://quench.forschung.kit.edu/82.php> (accessed on 30 January 2023).
9. Stuckert, J.; Grose, M.; Stegmaier, U.; Steinbrück, M. Results of Severe Fuel Damage Experiment QUENCH-15 with ZIRLOTM Cladding Tubes. In *Scientific Reports 7576*; KIT Scientific Publishing: Karlsruhe, Germany, 2011.
10. Stuckert, J.; Hollands, T.; Dolganov, K. Experimental and modeling results of the QUENCH-19 bundle tests with FeCrAl claddings. *IAEA Tecdoc Ser.* **2019**, *71*.
11. InProcess Instruments. *Gesellschaft für Prozessanalytik mbH, GAM 300 Process Analysis for Industrial Applications*; DB_GAM300-B/e, 01/2011; InProcess Instruments: Bremen, Germany, 2011.
12. Experimental Data Obtained in the Frame of the Project TAČR Théta TK03020034, Využití Pokročilých Materiálů pro Nové Typy Jaderného Paliva, no. iFIS 312-3122002D000. Available online: <https://starfos.tacr.cz/cs/project/TK03020034> (accessed on 30 January 2023).
13. Pint, B.A.; Terrani, K.A.; Brady, M.P.; Cheng, T.; Keiser, J.R. High temperature oxidation of fuel cladding candidate materials in steam–hydrogen environments. *J. Nucl. Mater.* **2013**, *440*, 420–427. [[CrossRef](#)]
14. Kim, C.; Tang, C.; Große, M.; Maengy, Y.; Jang, C.; Steinbrück, M. Oxidation mechanism and kinetics of nuclear-grade FeCrAl alloys in the temperature range of 500–1500 °C in steam. *J. Nucl. Mater.* **2022**, *564*, 153696. [[CrossRef](#)]
15. Pawel, R.E.; Cathcart, J.V.; McKee, R.A. The Kinetics of Oxidation of Zircaloy-4 in Steam at High Temperatures. *J. Electrochem. Soc.* **1979**, *126*, 1105–1111. [[CrossRef](#)]
16. Baker, L.; Just, L. Technical Report ANL-6548. *Argonne Natl. Lab.* **1962**. Available online: <https://www.osti.gov/biblio/4781681> (accessed on 30 January 2023).
17. Hollands, T.; Lovasz, L.; Gabrielli, F.; Carénini, L.; Luxat, D.L.; Phillips, J. Status of Modelling of FeCrAl Claddings in Severe Accident Cides and Application on the QUENCH-19 Experiment. In Proceedings of the 10th European Review Meeting on Severe Accident Research, Karlsruhe, Germany, 16–19 May 2022.

Disclaimer/Publisher's Note: The statements, opinions and data contained in all publications are solely those of the individual author(s) and contributor(s) and not of MDPI and/or the editor(s). MDPI and/or the editor(s) disclaim responsibility for any injury to people or property resulting from any ideas, methods, instructions or products referred to in the content.